Available online at www.sciencedirect.com
ScienceDirect
Lithos 91 (2006) 208–228
LITHOS
www.elsevier.com/locate/lithos

Fluid inclusions in apatite from Jacupiranga calcite carbonatites: Evidence for a fluid-stratified carbonatite magma chamber

Alessandra Costanzo [a,*], Kathryn Ruth Moore [a], Frances Wall [b], Martin Feely [a]

[a] Department of Earth and Ocean Sciences, National University of Ireland Galway, Galway, Ireland
[b] Department of Mineralogy, The Natural History Museum, London, SW7 5BD, UK

Received 2 August 2005; accepted 13 March 2006
Available online 21 June 2006

Abstract

Carbonatites of the Jacupiranga alkaline–carbonatite complex in São Paulo State, Brazil, were used to investigate mineral–fluid interaction in a carbonatite magma chamber because apatite showed a marked discontinuity between primary fluid inclusion-rich cores and fluid inclusion-poor rims. Sylvite and burbankite, apatite, pyrite, chalcopyrite and ilmenite are the common phases occurring as trapped solids within primary fluid inclusions and reflect the general assemblage of the carbonatite. The apatite cores had higher Sr and REE concentrations than apatite rims, due to the presence of fluid inclusions into which these elements partitioned. A positive cerium anomaly was observed in both the core and rim of apatite crystals because oxidised Ce^{4+} partitioned into the magma. The combined evidence from apatite chemistry, fluid inclusion distribution and fluid composition was used to test the hypotheses that the limit of fluid inclusion occurrence within apatite crystals arises from: (1) generation of a separate fluid phase; (2) utilization of all available fluid during the first stage of crystallization; (3) removal of crystals from fluid-rich magma to fluid-poor magma; (4) an increase in the growth rate of apatite; or (5) escape of the fluids from the rim of the apatite after crystallization. The findings are consistent with fractionation and crystal settling of a carbonatite assemblage in a fluid-stratified magma chamber. Secondary fluid inclusions were trapped during a hydrothermal event that precipitated an assemblage of anhedral crystals: strontianite, carbocernaite, barytocalcite, barite and norsethite, pyrophanite, magnesian siderite and baddeleyite, ancylite-(Ce), monazite-(Ce) and allanite. The Sr- and REE-rich nature of the secondary assemblage, and lack of a positive cerium anomaly indicate that hydrothermal fluids have a similar source to the primary magma and are related to a later carbonatite intrusion.

Keywords: Carbonatite; Apatite; Fluid inclusions; Magma chambers

1. Introduction

The importance of understanding fluid behaviour in carbonatitic magma is illustrated by the fact that it will dictate the extent of mantle metasomatism or fenitization, and strongly influence whether or not a carbonatite can ascend through the solidus ledge and 'take-off' to the Earth's surface (Bailey, 1985). Fluid inclusion studies enable investigation of fluid behaviour and fluid inclusions have been reported in a number of minerals within carbonatites: calcite, apatite monticellite, alkali feldspar, and forsterite (in phoscorite) (Aldous, 1986; Ting et al., 1994; Samson et al., 1995; Bühn and Rankin, 1999; Williams-Jones and Palmer,

* Corresponding author. Tel.: +353 91 493202; fax: +353 91 494533.
E-mail address: alessandra.costanzo@nuigalway.ie (A. Costanzo).

0024-4937/$ - see front matter © 2006 Elsevier B.V. All rights reserved.
doi:10.1016/j.lithos.2006.03.047

2002; Bühn et al., 2002). Previous studies indicate that primary fluid inclusion types have fluid compositions that include relatively simple aqueous inclusions (liquid + vapour), more complex aqueous inclusions containing a variety of trapped and/or daughter minerals, carbonate melts, carbonic inclusions comprising CO_2 or a mixture of various carbonate–silicate–salt–H_2O-bearing fluids, dense CO_2, trapped over a wide range of temperatures (Roedder, 1984; Ting et al., 1994). Apatite is a particularly favourable host for studying fluids in carbonatites since it typically hosts a variety of abundant fluid inclusions parallel to the *c*-axis, demonstrating the primary origin of the fluids that must have been trapped during crystal growth.

Apatite, calcite and pyrochlore from the carbonatite in the plutonic Jacupiranga Complex in São Paulo State, Brazil, contain fluid inclusions and provide a good opportunity to investigate time-progressive fluid behaviour in a carbonatite magma chamber because successive carbonatite intrusions within the complex have previously been interpreted in terms of order of intrusion (Gaspar and Wyllie, 1983b). The complex, an economically important Cretaceous anorogenic intrusion into Precambrian basement, flanking the Paraná Basin in Brazil (Fig. 1a), is a NNW-elongated intrusive body (Fig. 1b) dominated by jacupirangite, which is cross-cut and fenitized by a small carbonatite stock 1000 m long and 400 m wide (Fig. 1c) (Born, 1989). The intrusion consists of five successive carbonatite intrusions with distinctive compositions (Gaspar and Wyllie, 1983a,b). The southern intrusions are: C_1 (oldest) calcite carbonatite, C_2 dolomite carbonatite and C_3 calcite carbonatite; the northern intrusions are C_4 calcite carbonatite and C_5 (youngest) dolomite carbonatite (Gaspar and Wyllie, 1983a,b). Since the aim of this study is to investigate the main stage of the magma chamber, the samples analysed are all related to the main body of the intrusion (C_1 to C_3) and not to the later northern intrusions. The samples analysed are apatite calcite carbonatite (A), forsterite calcite carbonatite (B) and phoscorite (C) from intrusion C_1; pyrochlore–apatite calcite carbonatite (D) from intrusion C_2, and calcite carbonatite (E) from C_3.

Minerals commonly found accompanying calcite in Jacupiranga carbonatites are dolomite, apatite, magnetite, forsterite, serpentine, clinohumite, phlogopite, pyrite, pyrrhotite, galena, ilmenite, spinel, pyrochlore, baddeleyite, barite and perovskite (Melcher, 1966). The types of carbonatite are identified according to the proportions of non-carbonate phases (phlogopite, forsterite, magnetite and apatite) and rock texture. Irregular banding is a common feature of the carbonatites, defined most commonly by the minerals magnetite and/or apatite, or by alternate layers of magnetite- and apatite-rich carbonatite, and almost pure carbonate bands (Born, 1989). Dolomite is subordinate and occurs as small blebs and short stringers in the calcitic mass or in fine myrmekite-like arrays in calcite (Born, 1989). Apatite–magnetite mineralization associated with the early stages of carbonatite activity may be rich in niobium, usually in the mineral pyrochlore (Mariano, 1989), and zirconium, usually in the mineral baddeleyite (Kukharenko et al., 1965; Borondin et al., 1973; Kapustin, 1980).

Apatite, calcite and pyrochlore from carbonatite within, and metasomatised jacupirangite around, the Jacupiranga Complex contain fluid inclusions. This research focuses on the fluid inclusions in apatite because apatite is a key mineral in carbonatite crystallization: it forms as an early liquidus phase and can continue crystallizing through to the last stage of hydrothermal activity. Apatite is a common accessory mineral in carbonatites worldwide (Le Bas et al., 1976) and has exceptionally constant composition with low though significant concentrations of REE, Sr and Ba; (Kapustin, 1977) key trace elements for petrogenetic investigations. The main objective of this research is to investigate the relationship between coexisting (magmatic) fluid and carbonatite magma in a chamber, using compositional variation in zoned apatite, in relation to the distribution and composition of fluid inclusions. We hypothesize that the distribution of fluid inclusions restricted to the cores of apatite crystals could be due to: (1) changes in crystal growth rate; (2) separation of a fluid phase from the magma prior to final apatite growth; (3) the utilization of all available fluid during the first stage of crystallization; (4) removal of a crystal from a fluid-rich magma to a fluid-poor magma; and (5) escape of the fluids from the rim of large apatite crystals after crystallization. Detailed chemical analyses of apatite crystals and the associated REE mineralization from calcite carbonatite belonging to the southern intrusion, representing the main stage of the magma chamber, are presented here, and combined with fluid inclusion evidence in order to investigate the role of fluid in the petrogenesis of the Jacupiranga complex.

2. Analytical methods

Samples from apatite calcite carbonatite (A), forsterite calcite carbonatite (B), phoscorite (C), pyrochlore–apatite calcite carbonatite (D), and calcite carbonatite (E) were investigated using a variety of analytical

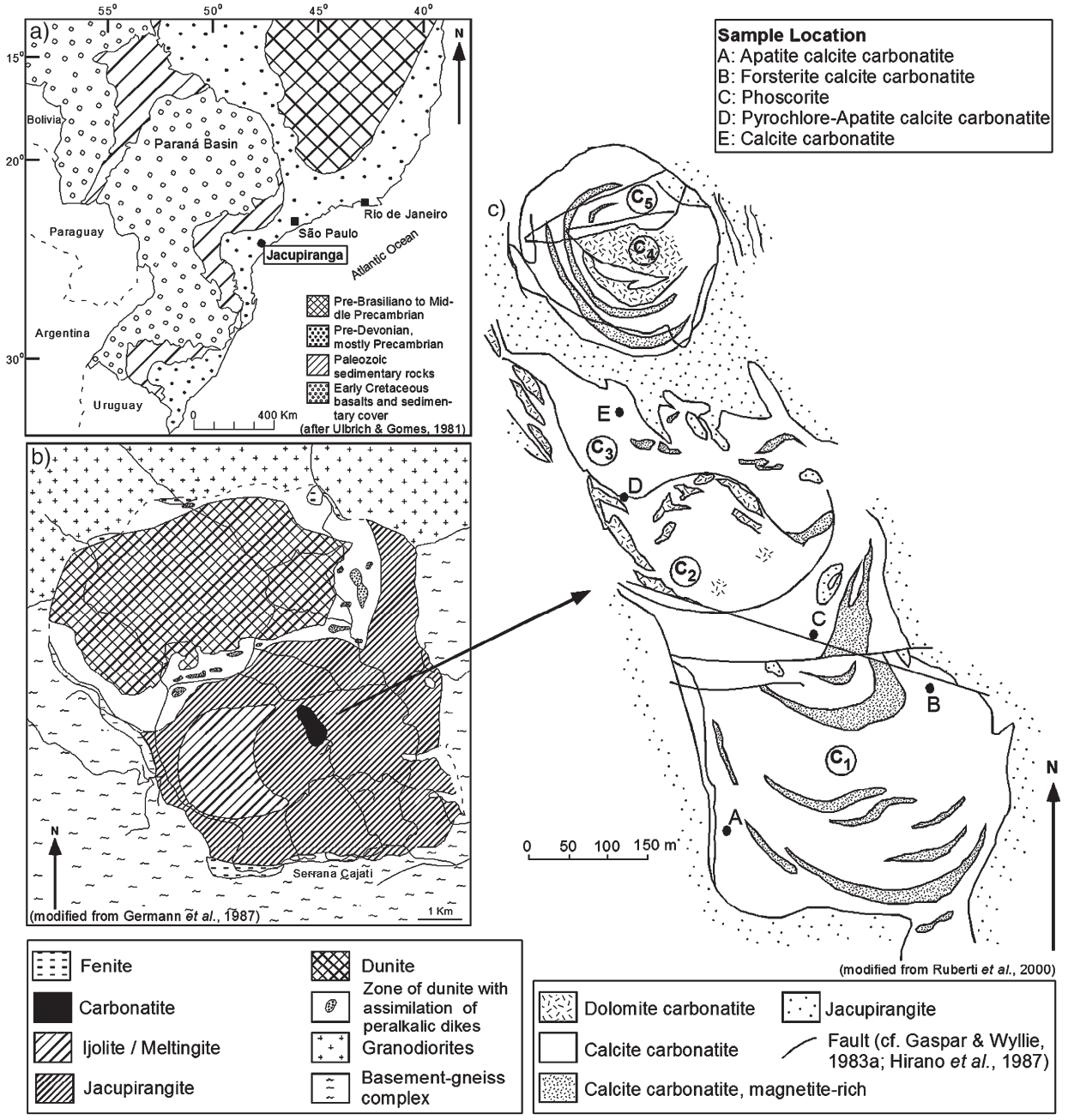

Fig. 1. Geological maps showing the location of the Jacupiranga Complex (a), the position of the carbonatite stock at the centre of the complex (b), and sample localities A–E (c) (after Ulbrich and Gomes, 1981; Germann et al., 1987; Ruberti et al., 2000). C_1–C_5 denote the order of intrusion: C_1, calcite carbonatite (oldest); C_2, dolomite carbonatite; C_3, calcite carbonatite; C_4, calcite carbonatite; C_5 dolomite carbonatite (youngest) (after Gaspar and Wyllie, 1983a,b; cf. Hirano et al., 1987).

techniques. Polished thin sections and wafers were prepared using an oil-based lubricating fluid in order to avoid any alteration of soluble carbonate. Qualitative investigations of composition using cathodoluminescence (CL), quantitative major element analysis using an electron microprobe (EPMA) and a Scanning Electron Microscope/Energy Dispersive Spectrometer (SEM/EDS), and quantitative trace element analysis using a Laser Ablation Inductively Coupled Plasma Mass Spectrometer (LA-ICP-MS), were carried out at the Natural History Museum in London. Laser Raman Microprobe (LRM) spectroscopy was carried out at the

School of Earth Sciences and Geography, Kingston University, London, and fluid inclusion microthermometric analyses were conducted at the Department of Earth and Ocean Sciences, National University of Ireland, Galway.

Wavelength-dispersive analyses, performed using a Cameca SX50 electron microprobe, used a variety of metal, natural and synthetic standards and a PAP matrix correction programme. Operating conditions were selected in order to minimize devolatilization: an accelerating voltage of 20 kV was combined with a beam current of ~20 nA and a 10–15 μm spot beam diameter. The lower detection limits were estimated as three times the standard deviation of the background count: 0.04 wt.% mean detection limit. The LA-ICP-MS analyses were performed using a Thermo Elemental Plasma Quad 3 ICP-MS coupled to a frequency quintupled Nd:YAG laser system operated at 213 nm. The laser had a beam diameter of 60 μm, and was fired at a repetition rate of 11 Hz with a pulse energy between 0.09 and 0.2 mJ per pulse. Four runs were made for each sample, consisting of 20 analyses per run. The first two and last two analyses in each run were made on the National Institute of Standards Technology (NIST) standard reference material NIST SRM 612, a silicate glass used for calibration. The concentration of calcium obtained from the electron microprobe was used to calibrate the ICP-MS analyses. EDS analyses were performed on a JEOL 5900LV scanning electron microscope equipped with an Oxford Instruments INCA energy dispersive X-ray microanalysis system and a Gatan cathodoluminescence detector. Operating conditions were 15 kV and 1 nA beam current measured on a vanadium calibration standard. Empirical corrections were made for REE elemental overlaps.

Cathodoluminescence petrography was carried out on a CITL Mk4 cold cathode system mounted on a Leica DML optical microscope and operated at 250 μA and 15 kV. Fluid inclusion petrography was completed using a transmitted light microscope and Lucia Archive Software linked to a digital camera. A confocal, multichannel Renishaw LRM (RM 1000) with an argon ion laser (514.5 nm) and thermoelectrically cooled CCD detector system was used to establish fluid inclusion gas, solid and liquid composition. The Laser Raman system was attached to an Olympus microscope with lens magnification up to 100×, enabling analysis of areas $\leq 4\ \mu m^2$ in size. The microprobe was calibrated regularly using a silicon standard to check and correct for any drift. Microthermometric analyses were performed on doubly polished wafers using a Linkam THMS-600 heating–freezing stage mounted on a Nikon Labophot transmission light microscope. The instrument equipped with a range of objective lenses including a 100× lens, was calibrated against synthetic H_2O (374.1 and 0.0 °C) and CO_2 (−56.6 °C) standards (Synthetic Fluid Inclusion Reference Set, Bubbles Inc., USA).

3. Calcite carbonatites from the southern intrusion of the Jacupiranga Complex

Calcite and dolomite dominate the mineral assemblages in the samples A–E (C_1 to C_3; Gaspar and Wyllie, 1983a,b), and are accompanied by apatite, magnetite, forsterite, phlogopite, pyrite and chalcopyrite in varying proportions (Fig. 2). Carbonatite has either a uniform granular texture or a rock foliation, defined by elongated grains of disseminated dolomite or sub-oriented apatite forming lenses up to several centimetres wide. Anhedral calcite crystals show a good cleavage, are commonly twinned and luminesce with a yellow-orange colour, while dolomite has an orange-red luminescence (Fig. 2c–f): dark red regions within the calcite are dolomite exsolution lamellae. Magnetite is also abundant and frequently found in rocks with a high apatite concentration. Ilmenite occurs both as lamellae in magnetite as well as isolated mineral grains. Phlogopite occurs in short light green zoned prismatic crystals and is occasionally found as inclusions in apatite crystals. Pyrochlore is the least abundant of the main rock-forming minerals and occurs only in parts of the complex, as yellow to brown dodecahedral crystals. Anhedral forsterite crystals up to 7 mm in size often contain inclusions of apatite and frequently have a rounded, irregular surface, due to corrosion or substitution by carbonates. Localized, large areas of the forsterite are serpentinised, particularly in cracks and along grain boundaries.

A complex assemblage of accessory phases includes pyrochlore, carbocernaite, ancylite-(Ce), barytocalcite, norsethite, pyrophanite, baddeleyite, zirconolite, burbankite, magnesian siderite and allanite (Fig. 3). The rare earth element and trace element rich phases, with the exception of zirconolite, occur as minute anhedral patches and are distributed within dolomite and apatite crystals (Fig. 3a, b), surroundings primary crystals (Fig. 3c–e), or within fractures traversing inclusions and infilled with the secondary REE-bearing minerals (Fig. 3f). Zirconolite occurs as euhedral crystals associated with phlogopite, enclosed within apatite (Fig. 3b). Crystals of strontianite, monazite-(Ce) and barite often occur in close proximity to magnetite, ilmenite and pyrite; sometimes as aggregates. Around the edge of apatite crystals, a halo of REE mineralization has been

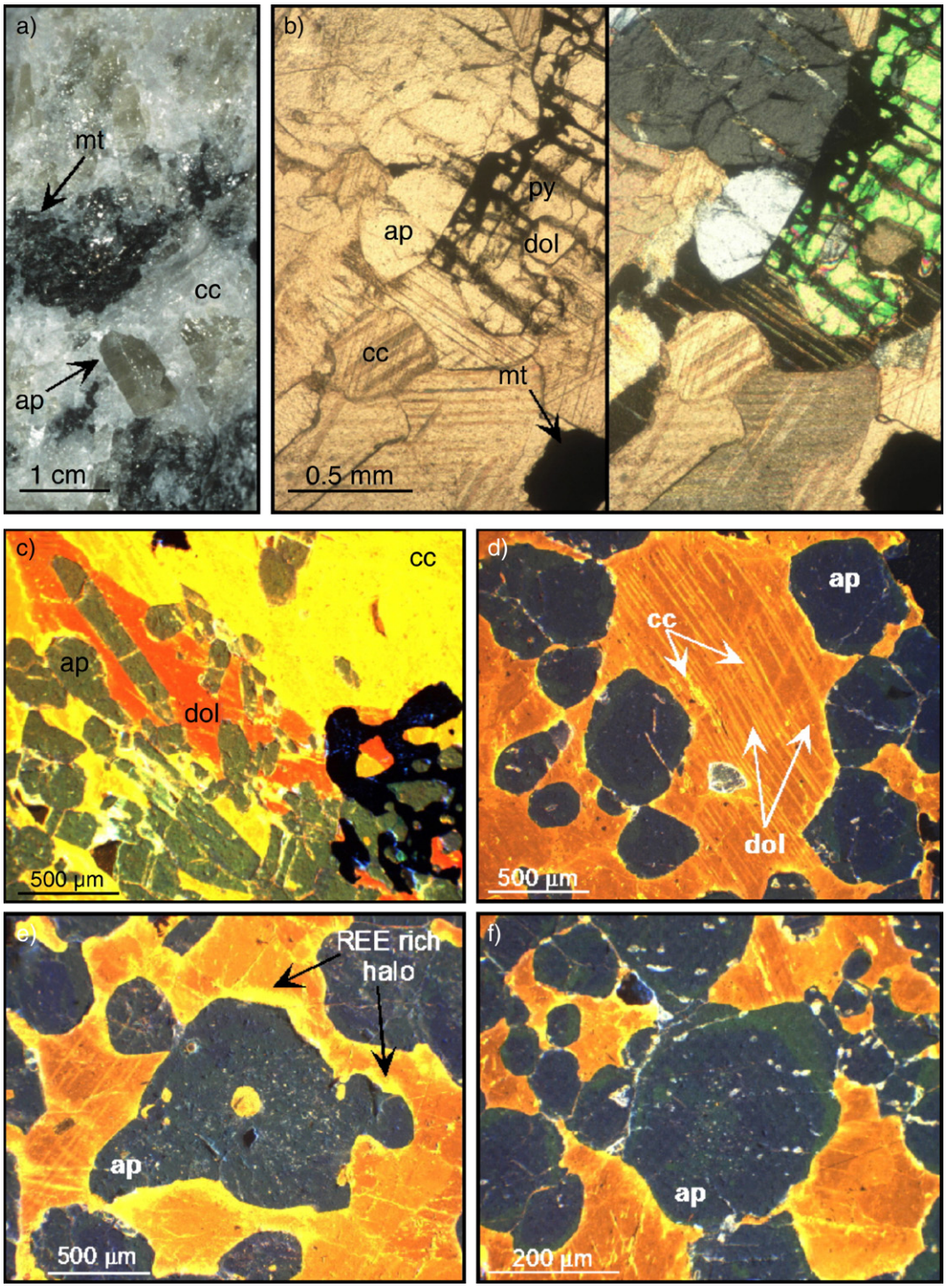

Fig. 2. Photograph (a) and photomicrographs (b–f; PPL on left, XPL on right) of carbonatite from the Jacupiranga Complex and cathodoluminescence (CL) photomicrographs of pyrochlore–apatite calcite carbonatite, sample D (c) and phoscorite, sample C (d–f) calcite (yellow) is easily distinguished from apatite (blue) and dolomite (orange) is recognised as crystals and as exsolution lamellae in calcite. Around the edges of apatite a halo of REE mineralization has been recognised within the dolomite. cc, calcite; ap, apatite; dol, dolomite; mt, magnetite; py, pyrochlore.

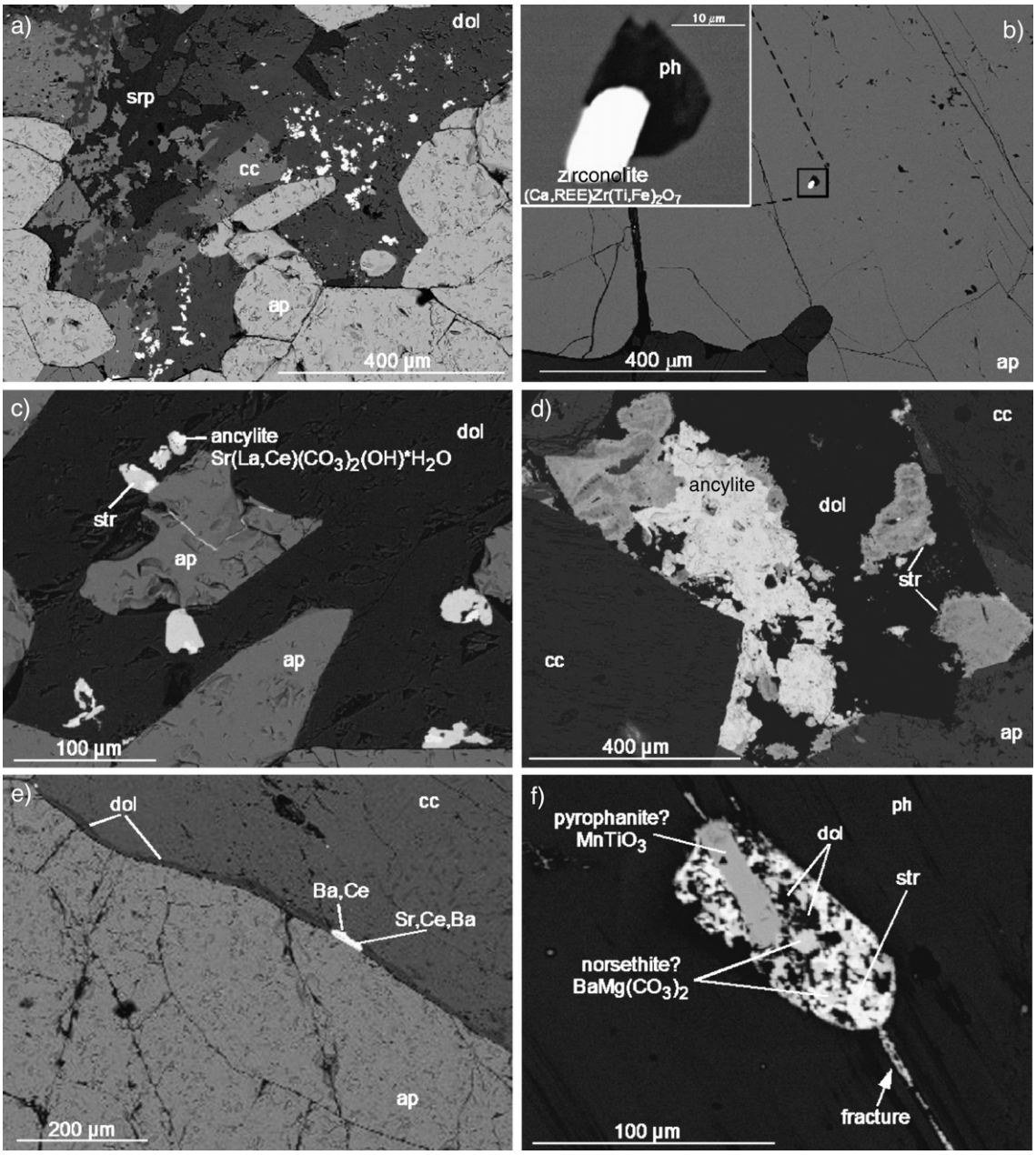

Fig. 3. BSE images showing REE mineralization in Jacupiranga carbonatite. Anhedral patches of ancylite and strontianite occur within dolomite crystals (a) and along the rim of apatite crystals (c, d) and are often characterized by minor replacement of Sr by Ca so that a marked rim is visible in strontianite to the right of image (d). Strontium-, REE-rich mineralization also occurs as minute anhedral patches within fractures of dolomite crystals, or along grain boundaries (e). In addition, secondary REE-bearing minerals can infill inclusions traversed by fractures (f). Primary REE-rich minerals are rare but euhedral zirconolite is observed with phlogopite as solid inclusions in apatite (b). cc, calcite; ap, apatite; dol, dolomite; srp, serpentine; str, strontianite; ph, phlogopite.

detected within the dolomite and appears as a yellow CL fringe (Fig. 2e).

Apatite is euhedral to subhedral and is evenly distributed within dense aggregations amongst the carbonates or in long sub-parallel idiomorphic prisms (up to 3 mm in length), forming lenses up to several centimetres thick (Fig. 4a). Petrographically, two types of apatite are distinguished. Apatite I is larger and elongated, closely associated with magnetite, phlogopite and pyrochlore, and contains numerous solid and aqueous inclusions confined exclusively in its core, in clearly delineated zones (Fig. 4a, b, c). Apatite II forms

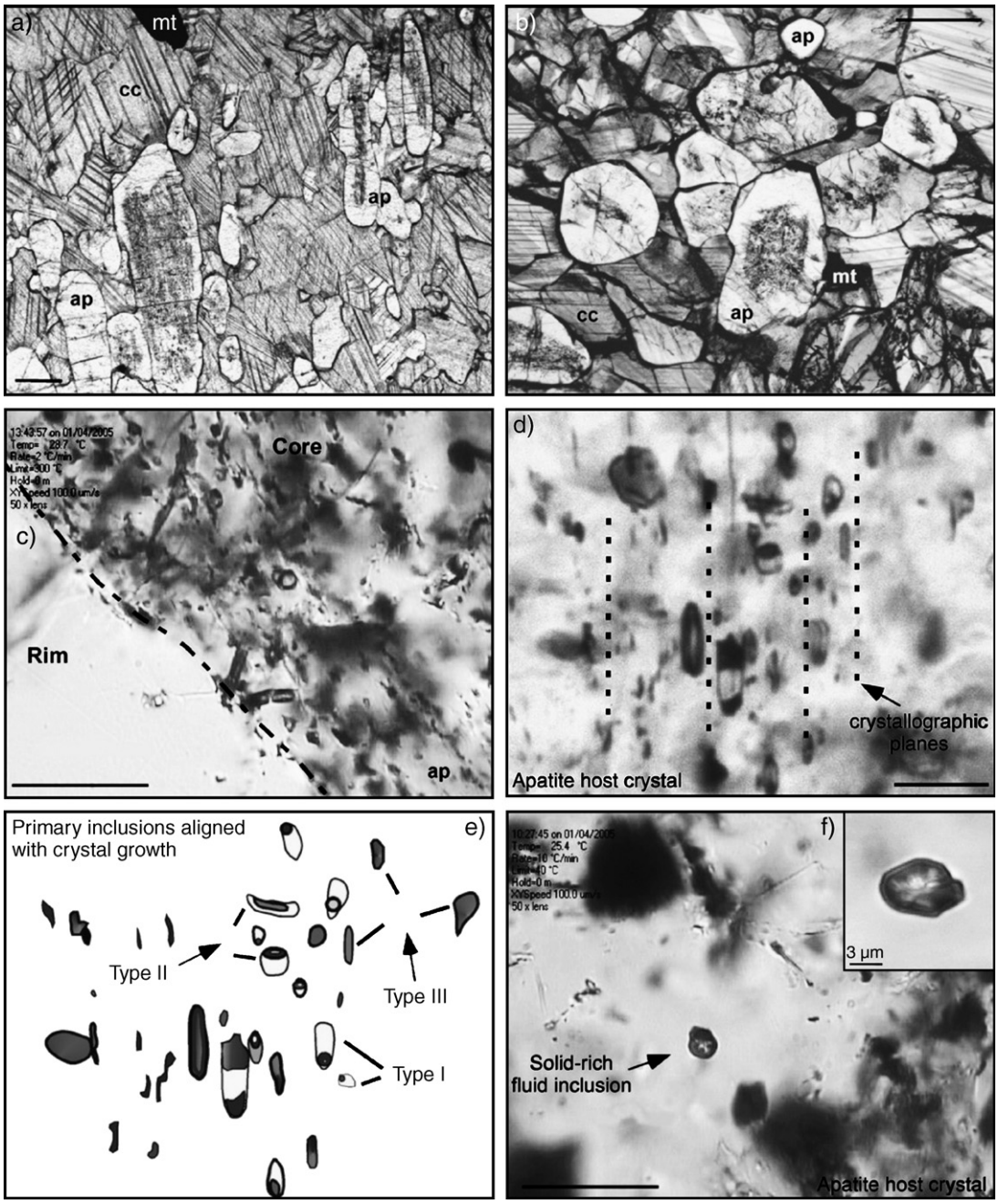

Fig. 4. Photomicrographs of elongate prisms (a) and ovoid apatites (b) in pyrochlore–apatite calcite carbonatite, sample D. A very sharp boundary divides the core and the rim in apatite crystals (c): the cloudy area in the core is due to the abundance of fluid inclusions. Fluid inclusions hosted in apatite, samples D and E are isolated solid-rich fluid inclusions (d–f) and aligned along the *c*-axis indicating they are primary in origin. cc, calcite; ap, apatite; mt, magnetite. Scale bar: 50 µm.

fine-grained clusters and streaks of smaller ovoid grains and is virtually free of fluid inclusions. Overall apatite concentration is variable, up to 40 modal % apatite. The quantity of fluid inclusions in apatite I is directly proportional to the size of the crystals. The width of the fluid inclusion-free outer zone ranges from 64 to 370 µm but is not constant in every crystal. Cathodoluminescence (Fig. 5) reveals several stages of growth of apatite crystals as crystals have a very mottled zonation. Bright luminescent zones within the core are

fluid-rich and are overgrown by a dull luminescent rim of apatite and some pale green luminescent patches and overgrowths at the margin of the crystals (Fig. 5a, b), consistent with manganese CL activation.

The apatite I crystals contain two different generations of solid carbonate inclusions. Large and rounded, slightly elongate crystals up to 350 μm in diameter (Fig. 5c, d) represent one type, in which single crystals are

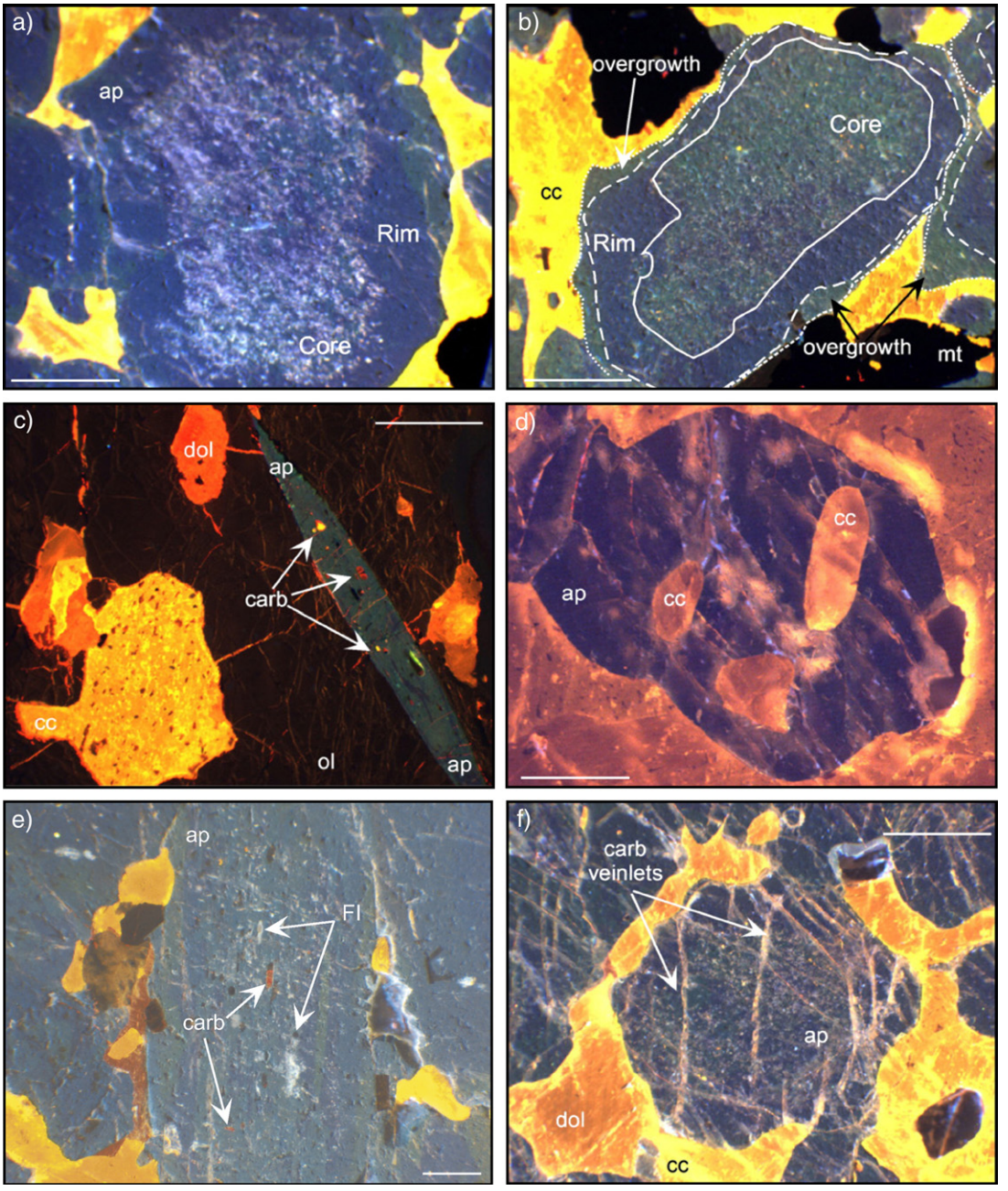

Fig. 5. Cathodoluminescence photomicrographs of apatite crystals from phoscorite (C) (a, b, e), apatite calcite carbonatite (A) (c, d) and forsterite calcite carbonatite (B) (f). Apatites (blue) with bright luminescent cores are fluid rich, overgrown by dull luminescing apatite rims and overgrowths (a–b). Single apatite crystals with elongate (yellow brown) carbonate inclusions (c), and fracture filling undetermined carbonate and calcite (d). Early-precipitated carbonate crystals are associated with aqueous fluid inclusions (FI) in the same apatite crystal core (e) and later numerous carbonate inclusions are closely associated with microfractures (f). cc, calcite; ap, apatite; dol, dolomite; mt, magnetite; ol, olivine; carb, carbonate. Scale bar: 500 μm.

mineral inclusions completely sealed within the apatites and interpreted as trapped crystals of early-precipitated calcite. They often occur side-by-side with primary aqueous inclusions in the same apatite crystal (Fig. 5e) but occasionally a small portion of aqueous fluid is actually trapped together with these calcite crystals. From the observations it is deduced that this calcite coexisted with the aqueous fluid (now preserved as aqueous inclusions) during the growth of the apatites. The second generation of solid carbonate inclusions is related to fracturing of apatite. Fluid inclusions breached by the fractures released their contents and the empty cavities are later infilled with secondary calcite or brownish/red ferruginous carbonate. Thus, small carbonate (yellow to white, Fig. 5f) veinlets connect secondary solid carbonate inclusions.

4. Fluid inclusion investigations

Fluid inclusions were classified into four different types (Table 1) according to the physical state of major phases present at room temperature, the dominant morphological features and the proportions of the major phases. Type I are liquid-rich aqueous inclusions (L+V) with a degree of fill between 0.75 and 0.90. Type II fluid inclusions are vapour-rich (usually H_2O), and the vapour bubble occupies more than half of the inclusion (V+L). Type III are monophase aqueous (L) or monophase vapour (V) inclusions. Type IV fluid inclusions contain one or more solid phases in addition to liquid or vapour and are subdivided into multiphase solid (MS) and multiphase multisolid (MMS) fluid inclusions. Type IV MS inclusions contain liquid, vapour and one crystal. Type IV MMS inclusions contain liquid, vapour and either more than one crystal of the same species or crystals of more than one mineral species.

The distribution of the fluid inclusions, as outlined by Shepherd et al. (1985), has been used to establish a paragenetic classification. Type I inclusions are identified as primary inclusions because they generally occur parallel to growth zones or crystal faces as prominent isolated inclusions at distances more than five times their diameter apart from one another, or distributed in linear arrays. Types II, III and IV are either secondary or pseudosecondary inclusions. Secondary fluid inclusions commonly occur in groups with curvi-linear distribution, outlining healed fractures. Pseudosecondary

Table 1
Classification scheme for fluid inclusions in the Jacupiranga carbonatites

Type	Physical state(s)		Composition	Typical examples
I	Liquid-rich, two-phase	L+V	L>50%	
II	Vapour-rich, two-phase	V+L	V=50% to 80%	
III	Monophase liquid	L	L=100%	
III	Monophase vapour	V	V≅100%	
IV	Multiphase solid	MS+L±V	S<50%	
IV	Multiphase multisolid	MMS+L±V	S>50%	

inclusions occur in planar groups that terminate abruptly within the crystal (Shepherd et al., 1985). The trails of small (4–24 μm) secondary and pseudosecondary inclusions (Types II, III and IV) cross-cut the earlier generations of larger (≤82 μm) Type I primary inclusions.

Fluid inclusions in the Jacupiranga carbonatitic rocks are hosted in crystals of apatite, calcite and pyrochlore. The calcite-hosted fluid inclusions were too small (<3 μm) for quantitative investigation. They occur as isolated MMS Type IV fluid inclusions or along healed microfractures, indicating that they are secondary. Pyrochlore likewise contains some fluid inclusions, Types I, II and III, distributed in linear arrays and rare isolated MMS Type IV fluid inclusions. In contrast, large fluid inclusions are abundant in the centre of apatite crystals with rounded, elongate or tubular shapes parallel to the *c*-axis of the mineral (Fig. 4d, e), i.e. trapped during primary growth of the crystal. Within a single apatite crystal, a variety of fluid inclusions with different L:V:S ratios may be trapped together as apparently primary inclusions.

Several analytical difficulties were encountered during microthermometric studies. Fluid inclusions were very small and lacked clarity, and leakage and decrepitation frequently occurred at relatively low temperatures (e.g. ~200 °C in apatite and between 250 and 327 °C in calcite), so characterization of fluid composition and behaviour could not easily be obtained by heating–freezing experiments. However, approximately one quarter of fluid inclusions (both primary and secondary) hosted in apatite did not leak or decrepitate and microthermometry revealed that the temperature of homogenization of primary fluid inclusions was greater than the 600 °C limits of the apparatus. Laser Raman microprobe (LRM) spectroscopy was used for the identification and non-destructive analysis of the crystalline solid phases (3–4 μm across) in Type IV

Table 2
Representative electron microprobe analyses (wt.%) of apatite

Rock	Fo calcite carbonatite-B (C_1)					Py–ap calcite carbonatite-D (C_2)				
Sample	#1	#8	#11	#19	#23	#1	#16	#70	#74	#75
Analysis	1	2	3	4	5	6	7	8	9	10
Na_2O	0.17	0.12	0.18	0.17	0.18	0.13	0.13	0.25	0.27	0.30
SiO_2	0.16	0.12	0.19	0.05	0.04	0.02	0.05	–	0.04	0.05
CaO	54.24	55.08	54.61	54.21	54.07	54.51	53.81	53.97	53.50	53.06
MnO	0.09	–	–	–	–	–	0.10	–	–	–
SrO	0.37	0.37	0.37	0.39	0.38	0.54	0.48	0.53	0.52	0.53
La_2O_3	–	–	–	–	0.13	0.11	–	0.10	–	–
Ce_2O_3	0.11	0.09	0.12	–	0.13	0.11	0.01	0.14	0.12	0.10
Nd_2O_3	n.a.	n.a.	n.a.	n.a.	n.a.	–	–	0.16	–	–
P_2O_5	41.97	42.72	42.91	42.50	42.16	42.88	41.10	41.50	41.75	41.49
F	2.21	1.92	1.90	2.12	1.90	0.82	0.66	0.70	0.68	0.62
Cl	n.a.	n.a.	n.a.	n.a.	n.a.	0.03	–	–	0.05	0.08
−O═F, Cl	0.93	0.81	0.80	0.89	0.80	0.35	0.27	0.28	0.31	0.30
Total	98.38	99.61	99.46	98.55	98.19	98.79	96.73	97.00	97.67	96.62
Structural formulae calculated on the basis of 25O										
Na	0.053	0.038	0.056	0.055	0.058	0.042	0.043	0.080	0.088	0.099
Ca	9.604	9.638	9.541	9.553	9.595	9.651	9.854	9.799	9.702	9.691
Mn	0.012	–	–	–	–	–	0.014	–	–	–
Sr	0.035	0.035	0.035	0.037	0.036	0.052	0.048	0.052	0.051	0.052
La	–	–	–	–	0.008	0.007	–	0.006	–	–
Ce	0.007	0.006	0.007	–	0.008	0.007	0.001	0.009	0.007	0.006
Nd	n.a.	n.a.	n.a.	n.a.	n.a.	–	–	0.010	–	–
P	5.873	5.906	5.924	5.918	5.912	5.999	5.947	5.953	5.983	5.988
Si	0.026	0.019	0.031	0.009	0.006	0.004	0.008	–	0.007	0.008
F	1.156	0.992	0.978	1.100	0.996	0.426	0.355	0.376	0.366	0.333
Cl	n.a.	n.a.	n.a.	n.a.	n.a.	0.009	–	–	0.014	0.023
Total	16.766	16.634	16.572	16.673	16.620	16.196	16.270	16.286	16.217	16.201
∑Cations	9.712	9.716	9.639	9.646	9.706	9.758	9.960	9.956	9.847	9.849
∑P+Si	5.899	5.925	5.955	5.927	5.918	6.003	5.955	5.953	5.989	5.996
∑F+Cl	1.156	0.992	0.978	1.100	0.996	0.435	0.355	0.376	0.381	0.356

Total Fe was calculated as FeO; –: below detection limit; n.a.: not analysed; Pr_2O_3, Nd_2O_3, Sm_2O_3, Y_2O_3 analysed are below detection limit.

inclusions (10–15 μm across) (Fig. 4e, f) and solids exposed on the broken surface of the host mineral were analysed by semi-quantitative SEM-EDX analysis. The individual solid phases were determined to be carbonate (e.g., calcite with the main Raman band at 1086 cm^{-1}). The most common mineral was sylvite but calcite and burbankite were also present, and non-carbonate minerals included apatite, pyrite, chalcopyrite and ilmenite. These minerals account for over 90% of the total assemblage, but unidentified phases are also present. LRM was also used to establish qualitatively the composition of the liquid and vapour phase in the fluid inclusions: only H_2O was detected. However, if the carbonate crystals precipitated from the cooling fluid within the inclusions, then the primary fluid, which may have subsequently leaked, must have contained carbon dioxide. The results imply that any CO_2 present was below the detection limit of the analytical techniques used or that all CO_2 was sequestered into solid phases. The presence of burbankite $(Na,Ca)_3(Sr,Ba,Ce)_3(CO_3)_5$, indicates that REE were an important component of primary fluids.

5. Apatite chemistry

Apatite is rich in strontium (0.35–0.55 wt.% SrO) and has low manganese (≤0.15 wt.% MnO), consistent with established carbonatitic apatite compositions. Major element compositions of the apatites are largely constant within any particular rock (Table 2), but apatite from forsterite calcite carbonatite (B) has slightly (~0.1 wt.%) less strontium and more than twice the fluorine concentration of apatite from pyrochlore–apatite calcite carbonatite (D). The apatite in assemblages containing pyrochlore is hydroxylapatite, with less than 1 wt.% fluorine, whereas apatite in assemblages containing olivine is hydroxyl-fluor-apatite, with up to 2 wt.% fluorine. There is no gradual change in chemistry across individual apatite crystals or evidence for zoning in terms of major element composition. However, there is a small but abrupt compositional change between the core and the rim of the crystal, as well as in the distribution of fluid inclusions (Fig. 4c). Average LA-ICP-MS analyses for selected trace elements of a number of crystals in apatite calcite carbonatite (A) and pyrochlore–apatite calcite carbonatite (D) are presented in Table 3, grouped according to petrographic characteristics. The abundance of fluid inclusions in apatite cores and the wide diameter of the beam (60 μm) used during LA-ICP-MS analyses indicate that compositions reported in Table 3 comprise both a fluid inclusions component and a host mineral component. Results show no significant difference between apatite I rims and apatite II crystals, and that

Table 3
Representative LA-ICP-MS analyses of selected trace elements in apatite from apatite calcite carbonatite (A) and pyrochlore–apatite calcite carbonatite (D)

	Apatite calcite carbonatite-A (C_1) oldest intrusion								Pyrochlore–apatite calcite carbonatite-D (C_2) youngest intrusion					
	Apatite I				Apatite II		Infilling carbonates		Apatite I				Calcite solid inclusion	
	Core $n=25$		Rim $n=10$		Fl-free crystals $n=15$		Fracture $n=4$		Core $n=33$		Rim $n=25$		$n=2$	
	Mean	S.E.	Mean	S.E.	Mean	S.E.	Mean	S.E.	Mean	S.E.	Mean	S.E.	Mean	S.E.
Mn	126.88	27.68	76.83	2.67	80.01	1.68	131.46	65.68	83.09	2.95	87.14	2.02	81.66	1.43
Sr	6779.85	266.40	5353.20	324.28	5084.56	232.82	8097.72	234.43	6403.00	96.71	6098.63	125.54	7322.93	827.29
Nb	0.80	0.51	0.26	0.03	0.65	0.18	0.41	0.22	0.30	0.05	0.23	0.02	0.07	0.01
Ba	69.29	20.65	23.96	0.93	26.17	0.69	133.94	87.71	48.28	4.73	25.07	1.13	36.79	1.99
La	330.40	13.25	279.41	17.26	291.36	10.64	314.44	18.16	283.57	6.70	228.00	4.80	347.84	0.85
Ce	930.87	49.25	858.42	92.67	1147.82	128.53	915.44	122.44	1125.37	59.17	654.78	31.48	1635.06	172.31
Pr	117.49	4.27	101.13	5.47	111.41	4.54	114.67	5.71	104.88	2.70	81.53	1.89	120.36	0.26
Nd	473.07	18.70	403.53	24.36	443.34	17.67	452.02	31.68	415.51	8.91	329.88	7.50	495.31	6.64
Sm	83.19	3.41	70.42	4.61	79.25	3.32	77.20	6.77	72.76	1.50	58.55	1.40	85.87	1.17
Eu	22.88	0.91	19.24	1.16	21.46	0.86	21.85	1.21	20.14	0.43	15.96	0.40	23.35	0.51
∑REE	2094.17	61.88	1857.38	117.44	228.45	152.07	2029.66	175.24	2142.11	78.60	1465.17	46.19	2842.65	162.37

Apatite I fluid inclusion-rich cores have higher trace element concentration than apatite I fluid inclusion-poor rims. Apatite II crystals have lower trace element concentrations except for cerium. Primary calcite solid inclusions have higher strontium and cerium concentrations than either apatite I or II crystals but secondary fracture-filling carbonate (calcite/dolomite) has higher strontium, barium and manganese concentrations than all other generations of minerals. n=number of analyses; S.E.: standard error.

apatite I rims (∑REEs of 0.16 wt.%; La:Yb=150:1 mol) have lower strontium concentration and slight LREE enrichment (Fig. 6a, b), compared to apatite I cores (∑REEs of 0.22 wt.%; La:Yb=155:1 mol). There is an overall decrease in rare earth element concentration from core to rim, but by far the most significant compositional variation observed in apatite crystals is a mean decrease in cerium concentration from core to rim of 13% (Table 3), which was observed in all crystals (n=20) that were systematically analysed, though a positive cerium anomaly is observed in both (Fig. 6a). The carbonate solid inclusions trapped in apatite during the early stage of crystallization (Table 3; solid inclusion) have very high cerium concentrations; they are first generation calcite inclusions, unrelated to fractures and subhedral in shape, indicating that trapping occurred early during crystal growth.

Fig. 7 shows a compositional transect across an apatite crystal: the fluid inclusion-rich core has a greater concentration of rare earth elements (for example, analyses 14–16) than the fluid inclusion-poor rim (analyses 1–2); rare earth element concentration in apatite is decreased in very close proximity to fractures (analysis 18) whereas fracture infilling is not depleted in rare earth elements and is enriched in cerium (analysis 5). Analyses 5 and 18 are both located within the fluid inclusion-rich core. The implication is that the rare earth elements reside partly in the fluid phase trapped as inclusions within the apatite and may be released by fracturing, though the zone of the apatite crystal affected by the fracturing is very narrow, and are then concentrated in secondary fluids. The narrowness of the zone of fluid inclusions of the apatite crystal affected by fracturing and the fact that fracturing cuts across apatite cores and rims in equal measure imply that fracturing cannot account for the width of the fluid inclusion-free rim, 64–370 μm wide.

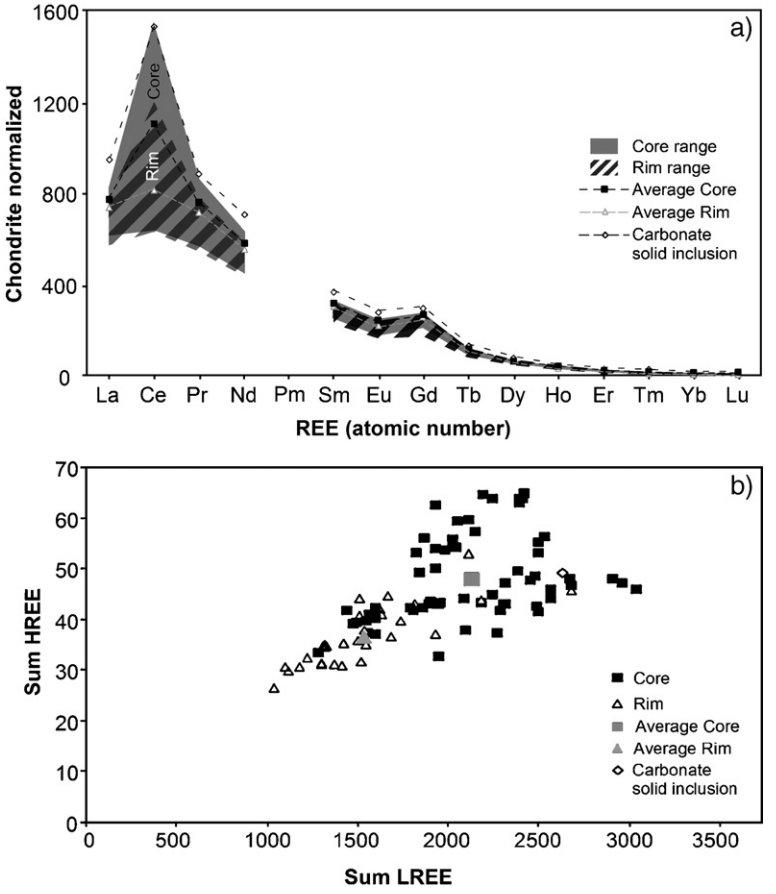

Fig. 6. Distribution of REE in apatite crystals from apatite calcite carbonatite (A) and pyrochlore–apatite calcite carbonatite (D). The REE distribution (a) is normalized using the chondritic values of Anders and Grevesse (1989). The shaded area gives the compositional range of all apatite I analyses: the darker area shows the composition of crystal cores while the lighter shading shows the composition of crystal rims (a). Apatite crystals have a LREE-enriched composition with decreasing total REE from core to rim (b).

6. Discussion

The salient points of apatite and fluid inclusion petrography and geochemistry are as follows. (1) Early REE-rich solids including zirconolite and calcite (Figs 3b and 5c respectively) were trapped alongside primary fluid inclusions in the core of apatite crystals. (2) An event occurred such that fluids no longer became trapped in the rim of crystals, though the major element chemistry of the apatite was unaffected and there were only minor differences in trace element chemistry (average REE difference, excluding Ce, from core to rim = 14 ppm). (3) There is evidence for later manganese-rich overgrowths (indicated by CL) on apatite, escape of fluids from inclusions through fractures, movement and exchange of REE along and across grain boundaries — particularly between apatite and dolomite, and re-precipitation and/or introduction of rare earth elements in accessory phases. Some or all of these later processes may have happened after consolidation of the magma. The generations of mineral growth are summarised in the paragenetic sequence shown in Table 4.

6.1. Apatite chemistry and zoning

The primary holocrystalline assemblage of calcite, dolomite, apatite and magnetite with a composition high in strontium and rare earth elements (and a high ratio of LREE to HREE) is characteristic of carbonatites as described by Kapustin (1980). Sodium-, calcium-, strontium- and barium-bearing carbonates such as burbankite and carbocernaite, present at Jacupiranga, are commonly associated with carbonatite (Kapustin, 1980; Wall and Mariano, 1996; Zaitsev et al., 1998). The ratio of strontium to manganese in both the core and the rim of apatite crystals from Jacupiranga is approximately Sr:Mn = 68:1 — it is of the same order of magnitude as in apatite crystals from other carbonatite complexes (Sr:Mn = 50:1; Brasseur et al., 1962). The Jacupiranga samples appear more strontium-rich than

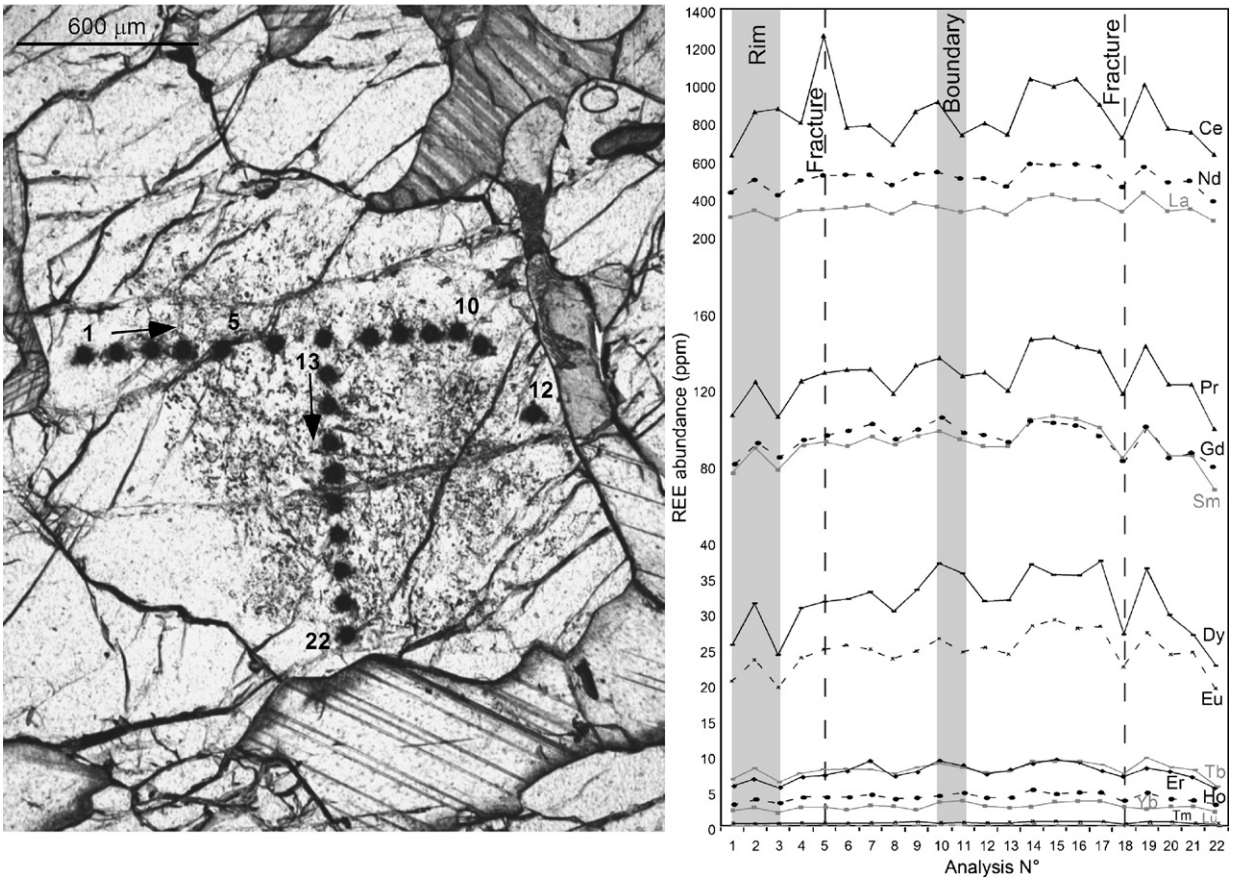

Fig. 7. Distribution of REE within an apatite crystal. A compositional traverse across a fractured apatite crystal in apatite calcite carbonatite, (A), shows that REE are present in greater concentrations in unfractured fluid inclusion-rich cores than in unfractured fluid inclusion-poor rims, are released from fluid inclusions in the core of the crystal by fracturing and remobilized in secondary fluids (see text for details).

Table 4
Simplified paragenetic sequence for the mineral assemblage in carbonatite from Jacupiranga

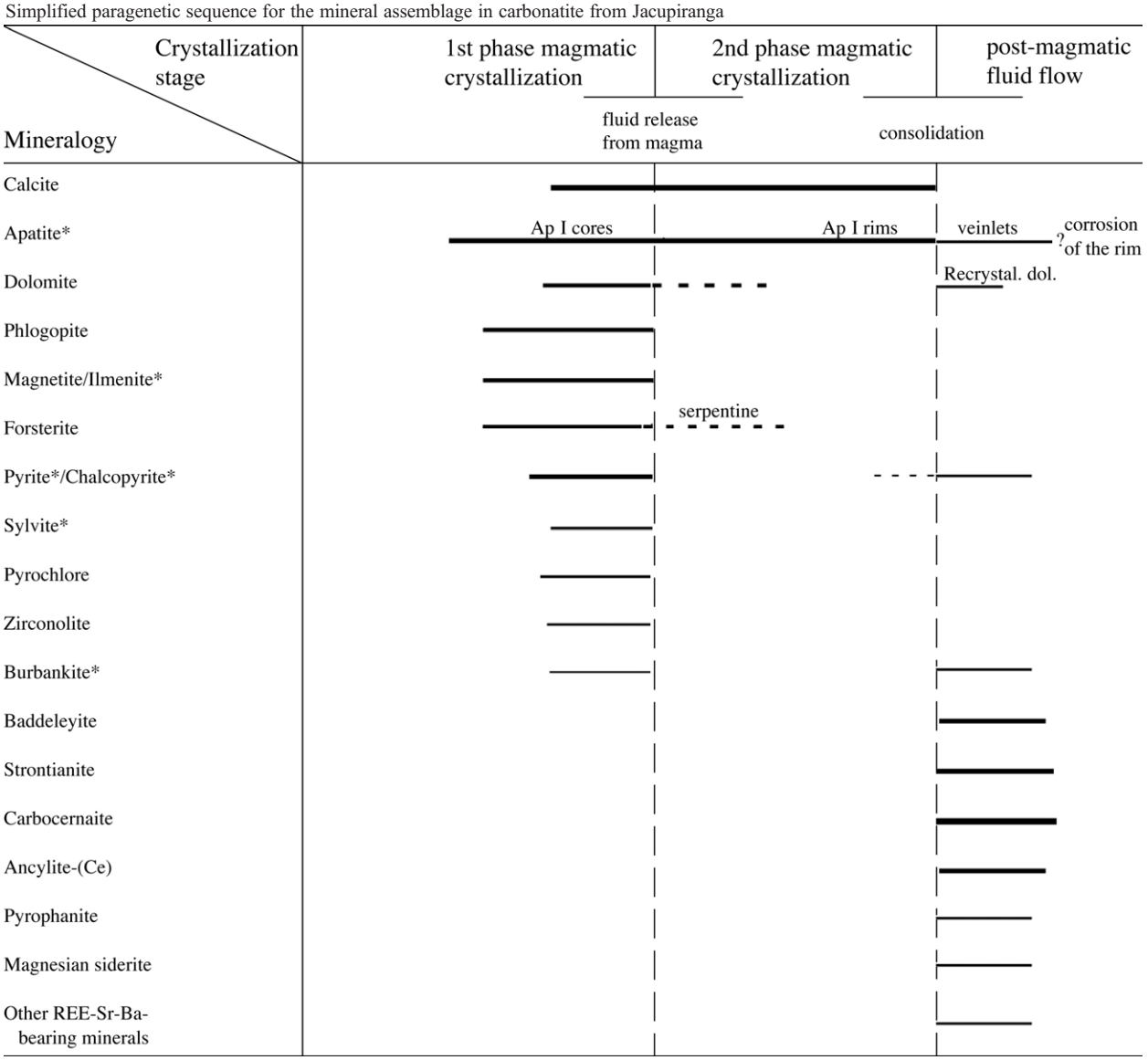

Table compiled using petrographic, fluid inclusion and chemical evidence for samples A to E. Other REE, Sr, Ba minerals include monazite-(Ce), baryte, barytocalcite, norsethite. Line thickness reflects the relative abundance of the minerals. Minerals marked with an asterisk occur as both primary crystals and as solid phases trapped in fluid inclusions.

the average (Brasseur et al., 1962), but the comparison does not take into account the abundance of coexisting strontium- and manganese-bearing phases. Apatite from Jacupiranga does not have major compositional zoning, unlike other localities (e.g.: Hogarth, 1989; Woolley et al., 1991; Le Bas et al., 1992; Karchevsky and Moutte, 2004; Wall, 2004), which is particularly significant for REE, strontium, manganese and sodium. The zoning is normally attributed to secondary alteration (Woolley et al., 1991; Le Bas et al., 1992), identified by pervasive zoning along cracks and crystal boundaries. In Jacupiranga samples, only a narrow margin (30–35 μm) of alteration in the form of REE-enrichment in dolomite (Fig. 2e) and depletion in apatite is observed along grain boundaries that can be attributed to the secondary movement of hydrothermal fluids. Alves and Hagni (2004) also ascribed the development of the bright outermost zone of some apatite crystals to hydrothermal alteration. They considered this hydrothermal event to be local, but significant enough to cause

recrystallization of grains of the carbonate minerals. The fluid inclusion-poor area (64 to 370 μm wide) of apatite crystals, containing the narrow margin of secondary alteration, shows no compositional zonation towards the crystal margins. Thus the lack of fluid inclusions in the apatite rims is not a secondary effect. Primary aqueous inclusions that occur as uniform elongate cavities along the *c*-axis within apatite crystals are common in many carbonatitic complexes (Rankin, 1975, 1977) but seldom described as restricted to the cores of apatite crystals (Samson et al., 1995; Williams-Jones and Palmer, 2002).

While there is no major element zoning and no gradual change in trace element chemistry in Jacupiranga apatites, there are small but measurable compositional differences between fluid inclusion-rich cores and fluid inclusion-poor rims of apatite. Most published accounts (Zaitsev and Bell, 1995; Bühn et al., 2001; Krasnova et al., 2004; Lee et al., 2004) of carbonatite complexes describe an increase in fluorine and strontium concentrations with growth of apatite crystals (Karchevsky and Moutte, 2004). The opposite trend is recorded for the apatite crystals from Jacupiranga – these decrease slightly during crystallization (Fig. 8) – and the most significant variation is a positive cerium anomaly, particularly in the core of apatite crystals (Fig. 6a), perhaps due to a transition from Ce^{3+} to Ce^{4+}. Weathering removes strontium and light rare earth elements from carbonatite, increases fluorine content and carbonation of apatite (Hogarth, 1989), and alteration processes cause oxidation of cerium (Le Bas et al., 1992). Weathering cannot account for the composition of Jacupiranga apatite rims as the samples were collected from the fresh outcrops of the Cajati mine and alteration affects apatite crystals only on grain boundaries. The Ce enrichment in Jacupiranga apatite was previously reported, though not accounted for, by Alves and Hagni (2004). It is now proposed that the positive cerium anomaly results from the oxidising effects (Irvine and Baragar, 1971; Best, 2003) of abundant fluids, which are typically water-dominated in association with carbonatite magma at shallow mantle and crustal pressures (Eggler, 1978). Fluid inclusion studies on Jacupiranga apatites concur that fluids are dominantly aqueous but with carbonate (burbankite and calcite) solids indicating the presence of same CO_2 in the fluid phase. CO_2-bearing fluids also occur at high oxygen fugacity (Pawley et al., 1992).

Apatite from various carbonatite complexes is often described occurring as solitary, rounded grains, or as veins and/or clusters of tightly-packed grains, and also exhibiting a variety of elongated inclusions within their

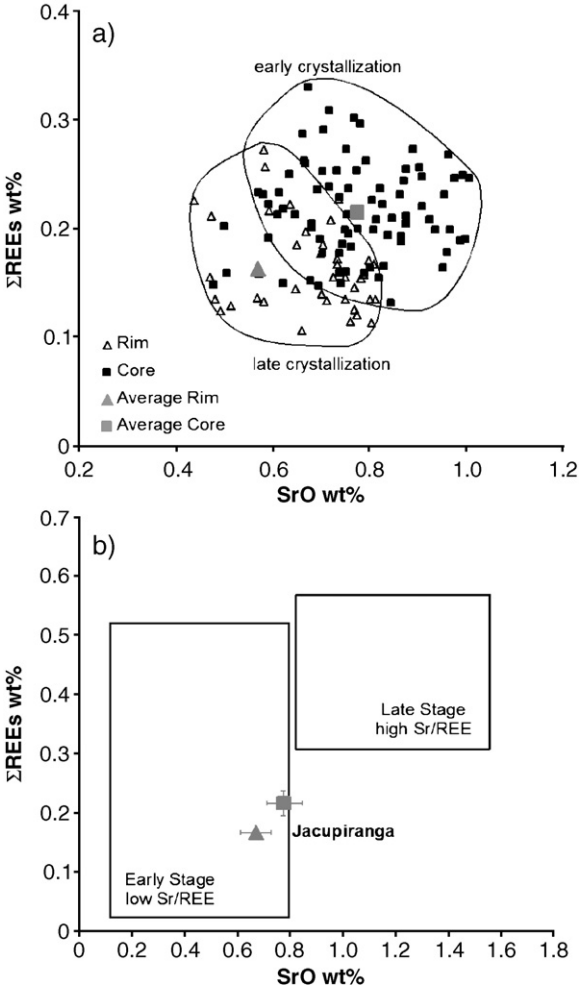

Fig. 8. Total REE against SrO wt.% for apatite I cores and rims in apatite calcite carbonatite, sample A (C_1), and pyrochlore–apatite calcite carbonatite, sample D (C_2). Analyses of crystals from both carbonatite samples show a consistent pattern of decreasing REE and strontium concentrations from fluid inclusion-rich cores to fluid inclusion-poor rims (a), though there is considerable overlap. The mean results for both core and rim lie within the reference field for early carbonatites (b) (Kapustin, 1977, 1982; Rimskaya-Korsakova et al., 1979).

cores. Inclusions consisting of rounded crystals of a highly birefringent mineral are common within apatite. Monocrystalline inclusions of calcite are relatively common in carbonatitic apatite (e.g. Girault, 1966; Rankin, 1975) and they have also been recognised in apatite from both Alnö and Usaki ijolites (Aspden, 1977, 1980). Solid inclusions classified as burbankite and khanneshite in hydroxylapatite were described by Zaitsev and Chakhmouradian (2002), as arranged in strings confined exclusively to the core of the crystals in Afrikanda complex, Kola Peninsula. The elongate

shape and pinch-off morphologies of early generation carbonate inclusions in Jacupiranga apatite have elsewhere been attributed to the liquid nature of the carbonate (Kogarko et al., 1995) at the time of entrapment. Fluid inclusions have been described confined to the core of apatite crystals from a variety of complexes e.g. in calciocarbonatite from Amba Dongar (Williams-Jones and Palmer, 2002), from Turiy Mys, Kola Peninsula (Dunworth and Bell, 2003), from Oka calcite carbonatite, Quebec (Samson et al., 1995), but there are no reported explanations for it.

6.2. REE distribution and phases of crystallization

The rare earth element distributions of most worldwide carbonatitic apatites are dominated by cerium, with Ce+La+Nd accounting for 80–85% (Kapustin, 1977). As with strontium, REE and fluorine, cerium concentration is decreased in the fluid inclusion poor-rim of Jacupiranga apatites, which predates the cerium-bearing secondary accessory assemblage (which has no Ce anomaly). Cerium is therefore an excellent means of differentiating between phases of crystallization. The cores of apatite I crystals are more REE-rich than apatite I rims and both have a positive cerium anomaly; apatite II crystals have the same positive cerium anomaly but higher concentration (Table 3); the late-stage separate mineral assemblage is very REE-rich but has no cerium anomaly. Secondary minerals rich in trace elements and rare earth elements, for example barite and monazite-(Ce) replace primary dolomite (Fig. 3a, c) but are contemporaneous with post-magmatic dolomite mineralization (Fig. 3e) at Jacupiranga.

Strontium in apatite generally increases from early to late carbonatite (Fig. 8): it enters calcite in early carbonatite but is concentrated in minerals such as barite and strontianite in later carbonatite intrusions (Hogarth, 1989). Sequestering in cerium-bearing ancylite-group minerals and strontianite at Jacupiranga corroborate the occurrence of subsolidus chemical re-equilibration. Ancylite has never been described as a magmatic mineral and is therefore taken to represent hydrothermal activity (Wall and Zaitsev, 2004). In Kola carbonatites such as Khibiny, Vuoriyarvi and Sallantavi, the most LREE-enriched compositions occur in the final magmatic rocks, and their immediate replacement pseudomorphs; REE and much of the fluid is sourced from the carbonatite itself (Zaitsev et al., 1998; Zaitsev and Chakhmouradian, 2002). Because Jacupiranga apatite cores and their associated fluid inclusions, and secondary (hydrous) mineralization (Table 4) both represent a high REE assemblage, it is likely that they had similar sources, i.e. the secondary cerium-minerals are associated with a hydrothermal fluid originating from a carbonatite magma later than that from which the apatite cores crystallized. The strontium- and REE-rich nature of the hydrothermal assemblage is also evidence that these elements partition more readily into the fluid phase than into magma. Preferential partitioning of REE into fluid and the lower concentrations of REE in apatite rims provide supporting evidence for the lack of availability of fluid in the carbonatite magma during apatite rim crystallization, indicated by the absence of fluid inclusions.

In general, carbonatitic apatite has highly variable total REE abundance (Hogarth, 1989), ranging from <1% ∑REE in some carbonatites to 8.3% in fluorapatite from the Chernigov carbonatite, Ukraine (Vil'kovich and Pozharitskaya, 1982). Apatite normally shows an increase in the LREE/HREE ratio from early to late carbonatite and this compositional trend may also apply from the core to the rim of individual crystals. Apatite crystals from the Jacupiranga calcite carbonatite have a relatively LREE-enriched composition and decreasing total REE from core to rim (Fig. 8). The $LREE_{ppm}/HREE_{ppm}$ ratio in Jacupiranga apatite decreases slightly from core to rim (mean $LREE/HREE_{core}=46$; mean $LREE/HREE_{rim}=41$). This is not a compositional change within the mineral but a reflection of the fact that fluids, into which REE preferentially partitions, are present in the cores i.e. the presence of fluids in the initial stage of crystallization. In Fig 8b, mean core and rim compositions are plotted alongside reference values for early and late stage carbonatite (Kapustin, 1977; Rimskaya-Korsakova et al., 1979; Kapustin, 1982). The composition of both rims and cores of apatite I crystals plot within the field of the early stage of crystallization, so that they represent early and late phases within a single crystallization event and overlap the Sr and REE values reported from various carbonatite complexes. This is in keeping with the field evidence that the southern intrusions C_1–C_3 are the earlier intrusions of the Jacupiranga Complex (Gaspar and Wyllie, 1983a,b) with lower reported strontium concentrations (0.47%; Alves and Hagni, 2004) than later intrusions of the Jacupiranga carbonatites (0.59–0.92%; Alves and Hagni, 2004).

6.3. Hypotheses of fluid entrapment in apatite

Mechanisms that may account for the apparent loss of a fluid phase include: (1) escape of the fluids from the rim of large apatite crystals after crystallization; (2) the

utilization of all available fluid during the first stage of crystallization; (3) changes in crystal growth rate; (4) separation of a fluid phase from the magma prior to final apatite growth; and (5) removal of a crystal from a fluid-rich magma to a fluid-poor magma.

The hypothesis that fluids escaped the apatite crystal rims after their crystallization is not supported by evidence from the rock samples. If fluid inclusions were being trapped at a consistent rate throughout the growth of the apatite crystal, then the rims would have been densely packed with fluid inclusions and it is unlikely that they would have disappeared entirely if emptied of fluid. For example, if natural decrepitation of fluid inclusions has occurred, empty dark cavities in the host crystal would be present. Field evidence undermines the hypothesis that all fluid was simply utilised early in the crystallization history of the magma chamber: successive intrusions (Gaspar and Wyllie, 1983a,b) show continued ascent of carbonatite magma from volatile-rich (Heinrich, 1966) sources, which would have continued to exsolve fluids due to the positive relationship between volatile solubility and pressure. Furthermore, if fluids were exsolved at a constant rate in the magma chamber, there is no reason that they should have all become trapped in early-formed crystals and many fluids should have remained within the magma for later stages of crystal growth.

A variation in the velocity of crystallization is possible and it may account for different growth conditions in the core and the rim of apatite, resulting in different modes of fluid entrapment, even if there is no change in the concentration of fluids present. Episodic increases in crystal growth rates, resulting from rapid temperature (or pressure) or fluid composition changes, or from deposition of foreign particles on the growing surface (cf. Voigt and Brantley, 1991), may lead to trapping of primary inclusions on the growth surface. Watanabe (1987) noted that inclusions were abundant on the fastest growing faces of corundum crystals, but were rare to absent on faces that grew more slowly. The simplest explanation, therefore, is that apatite initially grew quickly by undercooling, facilitating trapping of fluids along crystal defects, and subsequent slower crystallization permitted perfect apatite rim growth that excluded fluids. Primary fluid inclusions in Jacupiranga apatite occur both along growth planes and as large, isolated fluid inclusions, indicating that there could be rapid growth planes or points of nucleation for rapid growth during apatite I core crystallization but rapid undercooling of apatite results in skeletal, quench textured apatite (Wyllie et al., 1962), for which there is no evidence in the Jacupiranga apatites. Furthermore, some changes must have occurred within the system to cause the cessation of variable growth rates, to stop entrapment of fluids at the core–rim boundary. In other words, growth rate changes cannot be considered in isolation from other magma chamber processes.

The most likely causes for crystallization of a fluid inclusion free apatite rim are separation of a fluid phase from the magma prior to final apatite growth and removal of a crystal from a fluid-rich area of the magma chamber to a fluid-poor area of magma. The presence of the secondary assemblage in association with brittle fractures through crystals implies that the primary minerals resided in lithified rock prior to hydrothermal activity, which is therefore independent of separation of a fluid phase during apatite crystal growth. Evolution of a separate coherent fluid phase is possible if the volume of exsolved fluid relative to the volume of magma reached a critical level (Bailey, 1985). However, there is no apparent evidence of the movement of a vast amount of fluid through the surrounding country rock — metasomatic shells are observed on a scale of centimetres to tens of centimetres only.

6.4. Model for a fluid-stratified carbonatite magma chamber

The density of carbonatite magma at 1 bar and temperatures greater than 1100 °C is 2200 kg m^{-3} and the density of apatite is greater than 3000 kg m^{-3} (Treiman and Schedl, 1983). Settling rates are therefore rapid while upward magma flow rates in the centre of kilometre-sized intrusions are only of the order of 1 cm/s (Treiman and Schedl, 1983) though upward flow rates of fluid exsolved within the magma will be more rapid. Crystals larger than 0.5 mm could not therefore be suspended by the flow, and would settle to the bottom of a magma chamber (Treiman, 1989). As the fluid available is becoming concentrated at the top of the magma chamber, minerals common to carbonatite assemblages become concentrated at the bottom of the chamber, in a relatively fluid-poor magma. Thus, fluid inclusion-rich apatite cores may well have begun crystallization at or near the top of the magma chamber, growing as they settled (Fig. 9). As the quantity of fluid inclusions is directly proportional to the size of the crystal, it is likely the larger apatite I crystals simply settled through a greater height of fluid-rich magma. Small, fluid inclusion-free apatite II crystals with high Ce content (Table 3) may have been entirely crystallized in the lower portions of the magma chamber from where

oxidising fluids ascended. In the fluid-zoned crystals, the transition from core to rim is very abrupt. There is no decrease in the size or abundance of the fluid inclusions, implying that there was an abrupt level within the magma chamber at which fluid was exsolving and beginning to migrate upwards (Fig. 9). The partitioning of REE into fluids, the association of REE-rich fluids in the cores of apatite I crystals and the REE-rich nature of the secondary hydrothermal assemblage implies that the hydrothermal fluids have a carbonatite affinity. The secondary hydrothermal assemblage includes apatite and late-stage dolomite and is considered to be contemporaneous with dolomite mineralization at Jacupiranga reported by Born (1989). If the secondary REE-rich hydrothermal assemblage is contemporaneous with reported dolomite mineralization, then there are two possible sources for the hydrothermal fluid: (1) related to the last fraction of the early C_1–C_3 (Gaspar and Wyllie, 1983a,b) magmas, which became dolomite-rich by extensive calcite fractionation (Harmer and Wyllie, 1997); (2) they are fluids related to late stage carbonatite (C_5; Gaspar and Wyllie, 1983a,b) intrusions. The lack of a Ce anomaly in the secondary assemblage implies that hydrothermal fluids do not originate from the same magma that crystallized apatite, but from the later intrusions. This corroborates the view that the most LREE-enriched compositions occur in the final magmatic rocks and their immediate replacement pseudomorphs (Wall and Zaitsev, 2004).

7. Conclusions

Mineral analysis and fluid inclusion investigations were used to test hypotheses for formation of apatite crystals with fluid inclusion-rich cores and fluid inclusion-poor rims in carbonatite from the Jacupiranga Complex in São Paulo State, Brazil. The results showed that chemical variations in apatite crystals were related

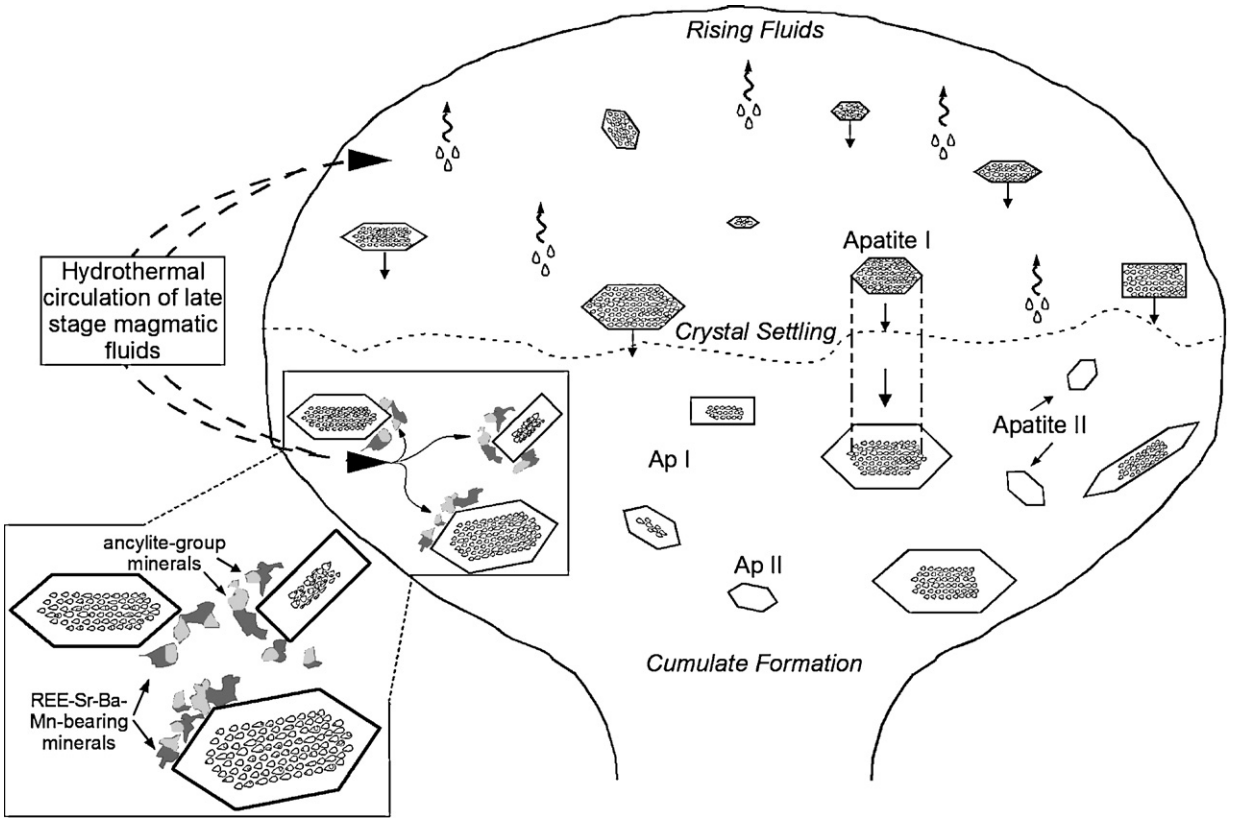

Fig. 9. Model for crystallization of apatite from carbonatite magma in a fluid-stratified magma chamber and REE–Sr–Ce minerals from hydrothermal fluids that affected the carbonatite after consolidation of cumulates. Primary fluid inclusions are trapped within the cores of apatite I crystal cores in the fluid-present portion of the magma chamber. Crystals continue to crystallize while settling through dry magma and form fluid inclusion-poor apatite rims. Apatite II crystallizes entirely within the dry portions of the magma chamber and contains few or no primary fluid inclusions. Secondary fluid inclusions are associated with the anhedral REE mineral and dolomite assemblage.

to the presence of fluid inclusions in the cores of the crystals, because Sr, REE and fluorine partition preferentially into the fluid phase, with the exception of Ce^{4+} which preferentially partitions into the magma. A positive cerium anomaly and REE enrichment in the apatite I cores, relative REE depletion in apatite I rims, high Ce concentration in apatite II and secondary REE-rich mineralization with no cerium anomaly allowed identification of a three-stage petrogenetic model. (1) Apatite crystals began to crystallize in the upper parts of a magma chamber, trapping associated magmatic fluid. (2) Apatite crystals settled through a fluid-stratified magma chamber and continued to crystallize from dry magma with higher Ce^{4+}. (3) Hydrothermal fluids from a later carbonatite magma source percolated through both the fluid inclusion-rich cores and fluid inclusion-poor rims of apatite crystals and other primary minerals, and crystallized a REE-rich anhedral mineral assemblage.

Acknowledgements

A. Costanzo acknowledges the financial support provided by the ACCORD Marie Curie training site and in particular Dr. F. Wall for the assistance received. We are grateful to Dr. C.T. Williams, Mr. A. Kearsley, Mr. J. Spratt and Mr. T. Wighton at the Natural History Museum and also Dr. Martin Smith, University of Brighton for their help and advice. The authors wish to acknowledge the advice and the assistance given with the LRM by Prof. Andrew Rankin in the School of Earth Sciences and Geography, Kingston University, London. K. Moore wishes to thank the Geological Society for the Daniel Pidgeon Fund to support field work and sample collection. The authors are grateful to Prof. Andrew Rankin and Dr. Anatoly Zaitsev for their insightful reviews that significantly improved the quality of this paper.

References

Aldous, R., 1986. Copper-rich fluid inclusions in pyroxenes from the Guide Copper Mine, a satellite intrusion of the Palabora Igneous Complex, South Africa. Economic Geology 81, 143–155.

Alves, P.R., Hagni, R.D., 2004. Bunge's Cajati Apatite Mine, SE Brazil: Mineralogy and Petrography of the Carbonatite Intrusions and the Relationship to Mineral Processing, ICAM-BR, São Paulo. Applied Mineralogy 653–656.

Anders, E., Grevesse, N., 1989. Abundances of the elements: meteoritic and solar. Geochimica et Cosmochimica Acta 53, 197–214.

Aspden, J.A., 1977. Inclusion studies in ijolites and carbonatitic rocks, with particular reference to the identification of the solid components Unpubl. Ph.D. thesis, Univ. Leicester. 220 pp.

Aspden, J.A., 1980. The mineralogy of primary inclusions in apatite crystals extracted from Alnö iolite. Lithos 13, 263–268.

Bailey, D.K., 1985. Fluids, melts, flowage and styles of eruption in alkaline ultramafic magmatism. Transactions of the Geological Society of South Africa 88, 449–457.

Best, M.G., 2003. Igneous and Metamorphic Petrology. Blackwell Science Publishing Ltd.

Born, H., 1989. The Jacupiranga Apatite Deposit, São Paulo, Brazil in Phosphate Deposits of the World. Phosphate Deposits of the World, Volume — Phosphate Rock Resources. Cambridge University Press, Cambridge, pp. 111–115.

Borondin, L.S., Lapin, A.V., Kharchenkov, A.G., 1973. Rare Metal Camaforites. Nauka, Moscow. 176 pp. (in Russian).

Brasseur, H., Herman, P., Hubaux, A., 1962. Apatites de l'est du Congo et du Ruanda. Annales de la Société Géologique de Belgique 85 (2), 61–85.

Bühn, B., Rankin, A.H., 1999. Composition of natural, volatile-rich Na–Ca–REE–Sr carbonatitic fluids trapped in fluid inclusions. Geochimica et Cosmochimica Acta 63 (22), 3781–3797.

Bühn, B., Wall, F., Le Bas, M.J., 2001. Rare-earth element systematics of carbonatitic fluorapatites, and their significance for carbonatite magma evolution. Contributions to Mineralogy and Petrology 141, 572–591.

Bühn, B., Rankin, A.H., Schneider, J., Dulski, P., 2002. The nature of orthomagmatic, carbonatitic fluids precipitating REE, Sr-rich fluorite: fluid-inclusion evidence from the Okorusu fluorite deposit, Namibia. Chemical Geology 186, 75–98.

Dunworth, E.A., Bell, K., 2003. The Turiy Massif, Kola Peninsula, Russia: mineral chemistry of an ultramafic–alkaline–carbonatite intrusion. Mineralogical Magazine 67 (3), 423–451.

Eggler, D.H., 1978. The effect of CO_2 upon partial melting of peridotite in the system Na_2O–CaO–Al_2O_3–MgO–SiO_2–CO_2 to 35 Kb, with an analysis of melting in a peridotite–H_2O–CO_2 system. American Journal of Science 278, 305–343.

Gaspar, J., Wyllie, P.J., 1983a. Magnetite in the carbonatites from the Jacupiranga Complex, Brazil. American Mineralogist 68, 195–213.

Gaspar, J., Wyllie, P.J., 1983b. Ilmenite (high Mg, Mn, Nb) in the carbonatites from the Jacupiranga Complex, Brazil. American Mineralogist 68, 960–971.

Germann, A., Marker, A., Friedrich, G., 1987. The alkaline complex of Jacupiranga. São Paulo. Brazil — petrology and genetic considerations. Zentralblatt für Geologie und Paläontologie 1, 807–818.

Girault, J., 1966. Genèse et géochimie de l'apatite et de la calcite dans les roches liée ou complex carbonatitique et hypercalin d'Oka (Canada). Bulletin Société Français de Minéralogie et de Cristallographie 89, 496–513.

Harmer, R.E., Wyllie, P.J., 1997. The origin of dolomitic carbonatites: field and experimental constraints. Journal of African Earth Sciences 25 (1), 5–28.

Hirano, H., Kamitani, M., Daitx, E.C., 1987. Jacupiranga carbonatites in the São Paulo State, Brazil: their mode of occurrence. Report of International Research and Development Cooperation ITIT Project, 8316, Japan, 74–95.

Heinrich, E.W., 1966. The Geology of Carbonatites. Rand McNally & Co, Chicago. 386 pp.

Hogarth, D.D., 1989. Pyrochlore, apatite and amphibole: distinctive minerals in carbonatite. In: Bell, K. (Ed.), Carbonatites: Genesis and Evolution. Unwin Hyman, London, pp. 105–148.

Irvine, T.N., Baragar, W.R.A., 1971. A guide to the chemical classification of the common volcanic rocks. Canadian Journal of Earth Sciences 8, 523–548.

Kapustin, Yu.L., 1977. Distribution of Sr, Ba, and the rare earths in apatite from carbonatite complexes. Geochemistry International 14 (4), 71–80.

Kapustin, Yu.L., 1980. Mineralogy of Carbonatites. Amerind Pub. Co, New Delhi. 259 pp.

Kapustin, Yu.L., 1982. Geochemistry of strontium and barium in carbonatites. Geochemistry International 19 (2), 38–48.

Karchevsky, P.I., Moutte, J., 2004. The phoscorite–carbonatite complex of Vuoriyarvi, northern Karelia. In: Wall, F., Zaitsev, A.N. (Eds.), Phoscorites and Carbonatites from Mantle to Mine: The Key Example of the Kola Alkaline Province. Mineralogical Society Series, vol. 10. Mineralogical Society, London, pp. 163–199.

Kogarko, L.N., Henderson, C.M.B., Pacheco, H., 1995. Primary Ca-rich carbonatite magma and carbonate–silicate–sulphide liquid immiscibility in the upper mantle. Contributions to Mineralogy and Petrology 121, 267–274.

Krasnova, N.I., Petrov, T.G., Balaganskaya, E.G., Garcia, D., Moutte, J., Zaitsev, A.N., Wall, F., 2004. Introduction to phoscorites: occurrence, composition, nomenclature and petrogenesis. In: Wall, F., Zaitsev, A.N. (Eds.), Phoscorites and Carbonatites from Mantle to Mine: The Key Example of the Kola Alkaline Province. Mineralogical Society Series, vol. 10. Mineralogical Society, London, pp. 45–74.

Kukharenko, A.A., Orlova, M.P., Bulakh, A.G., Bagdasarov, E.A., Rimskaya-Korsakova, O.M., Nefedov, E.I., Ilinskiy, G.A., Sergeev, A.S., Abakumova, N.B., 1965. The Caledonian Complex of Ultramafic, Alkaline Rocks and Carbonatites of the Kola Peninsula and Northern Karelia. Nedra, Leningrad, Russia. 772 pp. (in Russian).

Le Bas, M.J., Aspden, J.A., Woolley, A.R., 1976. Contrasting sodic and potassic inclusions in apatite crystals from an ijolite. Journal of Petrology 18, 248–262.

Le Bas, M.J., Keller, J., Kejie, T., Wall, F., Williams, C.T., Peishan, Z., 1992. Carbonatite dykes at Bayan Obo, Inner Mongolia, China. Mineralogy and Petrology 46, 195–225.

Lee, M.J., Garcia, D., Moutte, J., Williams, C.T., Wall, F., 2004. Carbonatites and phoscorites from Sokli Complex, Finland. In: Wall, F., Zaitsev, A.N. (Eds.), Phoscorites and Carbonatites from Mantle to Mine: The Key Example of the Kola Alkaline Province. Mineralogical Society Series, vol. 10. Mineralogical Society, London, pp. 133–162.

Mariano, A.N., 1989. Nature of economic mineralization in carbonatites and related rocks. In: Bell, K. (Ed.), Carbonatites; Genesis & Evolution. Unwin Hyman, London, pp. 149–176.

Melcher, G.C., 1966. The carbonatites of Jacupiranga, São Paulo, Brazil. In: Tuttle, O.F., Gittins, J. (Eds.), Carbonatites. Interscience, New York, pp. 169–181.

Pawley, A.R., Holloway, J.R., McMillan, P.F., 1992. The effect of oxygen fugacity on the solubility of carbon–oxygen fluids in basaltic melt. Earth and Planetary Science Letters 110, 213–225.

Rankin, A.H., 1975. Fluid inclusions studies in apatite from carbonatites of Wasaki area of western Kenya. Lithos 8, 123–136.

Rankin, A.H., 1977. Fluid inclusion evidence for the formation conditions of apatite from the Tororo carbonatite complex of Eastern Uganda. Mineralogical Magazine 41 (318), 155–164.

Rimskaya-Korsakova, O.M., Krasnova, N.I., Kopylova, L.N., 1979. Typochemism of apatites in the Kodvor complex deposit. Mineralogiya I Geokhimiya 6, 58–70 (in Russian).

Roedder, E., 1984. Fluid inclusions. Reviews in Mineralogy. Mineralogical Society of America 12 (664 pp.).

Ruberti, E., Gomes, C., Melcher, G.C., 2000. Geological and petrological aspects of the Jacupiranga alkaline–carbonatite association, southern Brazil. The Jacupiranga Carbonatite Complex (Part I) and the Poços de Caldas Alkaline Massif (Part II) — Minas Gerais and São Paulo States, Eastern Brazil.

Samson, I.M., Liu, W., Williams-Jones, A.E., 1995. The nature of orthomagmatic hydrothermal fluids in the Oka carbonatite, Quebec, Canada: evidence from fluid inclusions. Geochimica et Cosmochimica Acta 59 (10), 1963–1977.

Shepherd, T.J., Rankin, A.H., Alderton, D.H.M., 1985. A Practical Guide to Fluid Inclusion Studies. Glasgow and London, Distribuited in the USA by Chapman and Hall New York.

Ting, W., Burke, E.A.J., Rankin, A.H., Woolley, A.R., 1994. Characterisation and petrogenetic significance of CO_2, H_2O and CH_4 fluid inclusions in apatite from the Sukulu carbonatite, Uganda. European Journal of Mineralogy 6, 787–803.

Treiman, A.H., 1989. Carbonatite magma: properties and processes. In: Bell, K. (Ed.), Carbonatites—Genesis and Evolution. Unwin-Hyman, pp. 89–104.

Treiman, A.H., Schedl, A., 1983. Properties of carbonatite magma and processes in carbonatite magma chambers. Journal of Geology 91, 105–121.

Ulbrich, H.H.G.J., Gomes, C.B., 1981. Alkaline rocks from continental Brazil. Earth-Science Reviews 17, 135–154.

Vil'kovich, R.V., Pozharitskaya, L.K., 1982. Rare earth elements in calcite and apatite of the Chernigov zone. Geokhimiya 511–518 (in Russian).

Voigt, D.E., Brantley, S.L., 1991. Inclusions in synthetic quartz. Journal of Crystal Growth 113, 527–539.

Wall, F., 2004. An illustration of the evolution and alteration of carbonatites using REE, Sr-rich carbonatites at Nkombwa, Zambia. In: Vladykin, N.V. (Ed.), Proceeding of International Workshop in Deep-Seated Magmatism, its Sources and their Relation to Plume Processes, Ulan-Ude. Publishing House of the Institute of Geography SB RAS, pp. 48–67.

Wall, F., Mariano, A.N., 1996. Rare earth minerals in carbonatites: a discussion centred on the Kangankunde Carbonatite, Malawi. In: Jones, A.P., Wall, F., Williams, C.T. (Eds.), Rare Earth Minerals: Chemistry, Origin and Ore Deposits. Mineralogical Society Series, vol. 7. Mineralogical Society, London, pp. 193–225.

Wall, F., Zaitsev, A.N., 2004. Phoscorites and Carbonatites from Mantle to Mine: the Key Example of the Kola Alkaline Province. In: Wall, F., Zaitsev, A.N. (Eds.), Mineralogical Society Series, vol. 10. Mineralogical Society, London. 498 pp.

Watanabe, K., 1987. Inclusions in flux-grown crystals of corundum. Crystal Research and Technology 22, 345–355.

Williams-Jones, A.E., Palmer, D.A.S., 2002. The evolution of aqueous-carbonic fluids in the Amba Dongar carbonatite, India: implications for fenitisation. Chemical Geology 185, 283–301.

Woolley, A.R., Barr, M.W.C., Din, V.K., Jones, G.C., Wall, F., Williams, C.T., 1991. Extrusive carbonatites from the Uyaynah area, United Arab Emirates. Journal of Petrology 32 (6), 1143–1167.

Wyllie, P.J., Cox, K.G., Biggar, G.M., 1962. The habit of apatite in synthetic systems and igneous rocks. Journal of Petrology 3 (2), 238–243.

Zaitsev, A., Bell, K., 1995. Sr and Nd isotope data of apatite, calcite and dolomite as indicators of source, and the relationships of phoscorites and carbonatites. Contributions to Mineralogy and Petrology 121, 324–335.

Zaitsev, A.N., Chakhmouradian, A.R., 2002. Calcite–amphibole–clinopyroxene rock from the Afrikanda complex, Kola Peninsula, Russia: mineralogy and a possible link to carbonatites: II. Oxysalt minerals. The Canadian Mineralogist 40, 103–120.

Zaitsev, A.N., Wall, F., Le Bas, M.J., 1998. REE–Sr–Ba minerals from the Khibina carbonatites, Kola Peninsula, Russia: their mineralogy, paragenesis and evolution. Mineralogical Magazine 62, 225–250.